PAPER

Single-crystalline graphene radio-frequency nanoswitches

IOP Publishing Journal of Micromechanics and Microengineering

J. Micromech. Microeng. **25** (2015) 075022 (6pp) doi:10.1088/0960-1317/25/7/075022

Single-crystalline graphene radio-frequency nanoswitches

Peng Li[1,2] **and Tianhong Cui**[2]

[1] State Key Laboratory of Precision Measurement Technology and Instruments, Department of Precision Instruments, Tsinghua University, Beijing 100084, People's Republic of China
[2] Department of Mechanical Engineering, University of Minnesota, Minneapolis, MN 55455, USA

E-mail: tcui@me.umn.edu

Received 31 January 2015, revised 21 April 2015
Accepted for publication 8 May 2015
Published 18 June 2015

Abstract

Growth of monolayer single-crystalline graphene (SCG) using the low-pressure chemical vapor deposition method is reported. Graphene's superb quality and single-crystalline nature were characterized and verified by Raman microscopy, atomic force microscopy, and carrier mobility measurement. Radio-frequency (RF) nanoelectromechanical switches based on coplanar waveguide double-clamped SCG membrane were achieved, and the superb properties of SCG enable the switches to operate at a pull-in voltage as low as 1 V, with switch time in the nanosecond regime. Owing to their single-crystalline nature, the switches' lifetime (>5000 times) is much longer than that of polycrystalline graphene ones reported. The RF devices exhibit good isolation (−30 dB at 40 GHz (Ka band)), which can be further improved by SCG's conductivity variation due to actuation voltage.

Keywords: graphene, MEMS, RF switch

S Online supplementary data available from stacks.iop.org/JMM/25/075022/mmedia

(Some figures may appear in colour only in the online journal)

1. Introduction

Nanoelectromechanical systems (NEMS) is a rapidly growing research field for promising applications, for instance NEMS switches [1], resonators [2], etc. Radio-frequency (RF) NEMS switches, with ideal zero dc off-current and superb isolation at high frequency [3], could replace existing metal-oxide semiconductor (MOS) switches with intrinsic drawbacks such as high power dissipation and inferior high-frequency performance [4]. To expand the applications of RF NEMS switches, their moving parts should be further scaled down to decrease operation voltage and increase switching speed [1]. However, the properties of conventional bulk-silicon-based materials for RF NEMS switches drastically degrade when their thickness reaches nanoscale. Graphene, a 2D honeycomb crystal material with sp^2-bonded carbon atoms [5], is predicted to be an excellent candidate for RF NEMS switches owing to its extremely small thickness, superb in-plane stiffness [6], very low mass, and good conductivity [7].

Chemical vapor deposition (CVD) methods with copper substrate have been widely used to synthesis large-area monolayer graphene with relatively low cost in recent years [7–13]. Nevertheless, large area graphene film prepared by currently available growth methods is polycrystalline [14, 15]. Because of grain boundaries, most of graphene's electrical and mechanical properties dramatically degrade [16–18], having a detrimental effect on the performance of graphene devices. For instance, polycrystalline graphene dc NEMS switches can only operate about 4–5 times before breakdown due to the mechanically weaker grain boundary [1]. Therefore, single-crystalline graphene (SCG) NEMS are highly desired.

Graphene RF NEMS switches are predicted to have superb performance [19, 20]. Moreover, they are suitable for integration with graphene RF nanoelectronics, which are promising candidate for future all-graphene transceivers. Nevertheless, a high-performance graphene RF NEMS switch has not been realized so far. Here we report on a SCG RF NEMS switch integrated with coplanar waveguide. The SCGs were derived

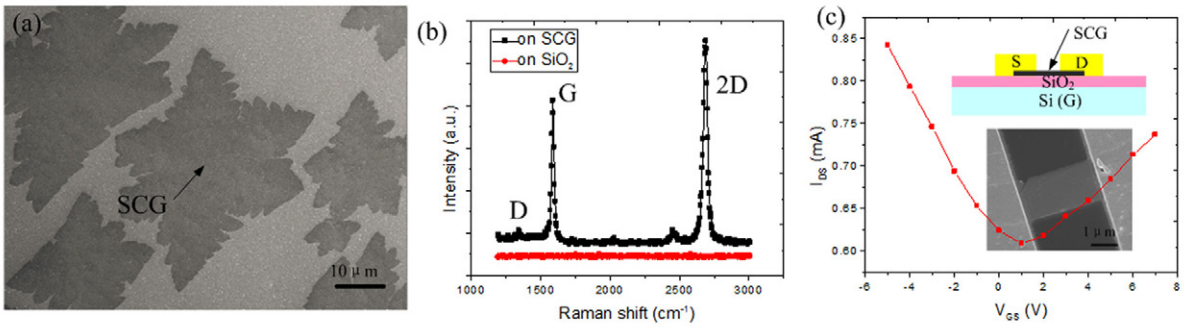

Figure 1. (a) Scanning electron microscopy (SEM) image of SCGs on copper foil. (b) Raman spectra derived on SCG and SiO_2 substrate, respectively. (c) I_{DS} versus V_{GS} of an SCG FET. The gate can cause either electron or hole conduction with transition point at V_{GS} =1V. The insets are schematic view and SEM image of SCG FET, respectively.

from low-pressure chemical vapor deposition (LPCVD) by controlling the growth duration. A new coplanar waveguide structure was proposed to avoid the metal fence effect [21] during device fabrication. The SCG RF NEMS switches exhibit small pull-in voltage (1 V) and superb switch speed (nanosecond regime), isolation (−30 dB at 40 GHz), and lifetime (>5000 times).

2. Experiment, results and discussion

LPCVD growth was carried out in a 2 in. quartz tube furnace on polycrystalline copper substrates (25 μm thick, 99.8%, Alfa Aesar) with a mixture of research-grade methane (as the carbon source) and hydrogen. Prior to growth, the copper foil was pretreated by diluted nitric acid to get rid of native oxide on the copper substrate for better growth. Copper foil was quickly loaded into the CVD furnace and pumped down to base pressure (<5 mTorr). Then the furnace was refilled with hydrogen and heated up to 1050 °C. Next, the sample was annealed to further remove the copper oxide. The growth was then carried out under a gas mixture of methane and hydrogen. Finally, the sample was cooled to room temperature rapidly without changing the gas flow rate. During growth, graphene grains initially nucleate from random locations. Then the growth of such SCG grains proceeds, and these grains eventually form a polycrystalline film. The grain boundaries of a continuous polycrystalline graphene film are invisible under optical microscope, so the growth was stopped before isolated SCG islands connected to each other to avoid grain boundary during device fabrication. Most of the monolayer SCG grains derived from LPCVD have star-like shapes (figure 1(a)). Decreasing methane flow rate can reduce nucleation density effectively, resulting in larger grain size. With appropriate growth parameters, SCG grains can easily reach tens of micrometers, large enough to be tailored to single or multiple NEMS devices.

After LPCVD growth, SCGs were transferred from copper foil onto a Si substrate with 300 nm SiO_2 on top by a PMMA (polymethyl methacrylate) -assisted process [2]. In order to remove PMMA residues [22] which may affect the performance of SCG devices, the sample was heated up to 300 °C at low pressure for 3 h. SCGs were characterized by Witec Alpha300R Confocal Raman microscope. D (~1350 cm^{-1}), G (~1580 cm^{-1}) and 2D (~2680 cm^{-1}) peaks were investigated. Number of graphene layers and defects inside graphene were verified by 2D/G peak intensity ratio and D peak intensity, respectively. The Raman spectrum derived from the SCG (figure 1(b)) demonstrates typical features of monolayer graphene: 2D peak > G peak and a sharp and symmetric 2D peak centered at ~2680 cm^{-1}. A negligibly small D peak over most of the area within a graphene grain was demonstrated in figure S1(a) (see the online supplementary information) (stacks.iop.org/JMM/25/075022/mmedia), indicating the low-defect and single-crystal nature of our sample, because defects and grain boundary are responsible for a prominent D peak in the Raman spectrum. Good uniformity of the SCG thickness was indicated by the 2D/G peak intensity ratio image shown in the online figure S1(c) (stacks.iop.org/JMM/25/075022/mmedia).

The morphology of SCG was investigated by atomic force microscope (AFM). The AFM topographic image displayed in the online figure S2(a) (stacks.iop.org/JMM/25/075022/mmedia) is presented without filtering or smoothing. The roughness of the surface was characterized by the standard deviation ρ of the height distribution and the height correlation length ℓ (see the online figure S2(b)) (stacks.iop.org/JMM/25/075022/mmedia), which are about 170 pm and 30 nm, respectively, close to the values of monolayer graphene on SiO_2 reported by Lui *et al* [23]. Carrier mobility measurement is widely used to evaluate the quality of graphene. SCG field-effect transistors (FETs) were fabricated with the SiO_2/Si substrate serving as the gate dielectric and the back gate. The drain–source current I_{DS} versus gate-source voltage V_{GS} curve exhibited an ambipolar behavior. Electron/hole conduction shifted at a transition point (Dirac point) of V_{GS} =1V (figure 1(c)). The carrier mobility of graphene can be deduced from [24]

$$\mu = \frac{\Delta I_{DS}}{C_{OX}\frac{W}{L}V_{DS}\Delta V_{GS}}, \quad (1)$$

where L and W are FET length and width, respectively, $C_{OX} = \varepsilon_{OX}\varepsilon_0 t_{OX}$ is gate oxide capacitance (ε_{OX} = 3.9 for silicon dioxide, ε_0 is vacuum permittivity, and t_{OX} is gate oxide thickness). A carrier mobility of 6208 $cm^2V^{-1}s^{-1}$ is derived.

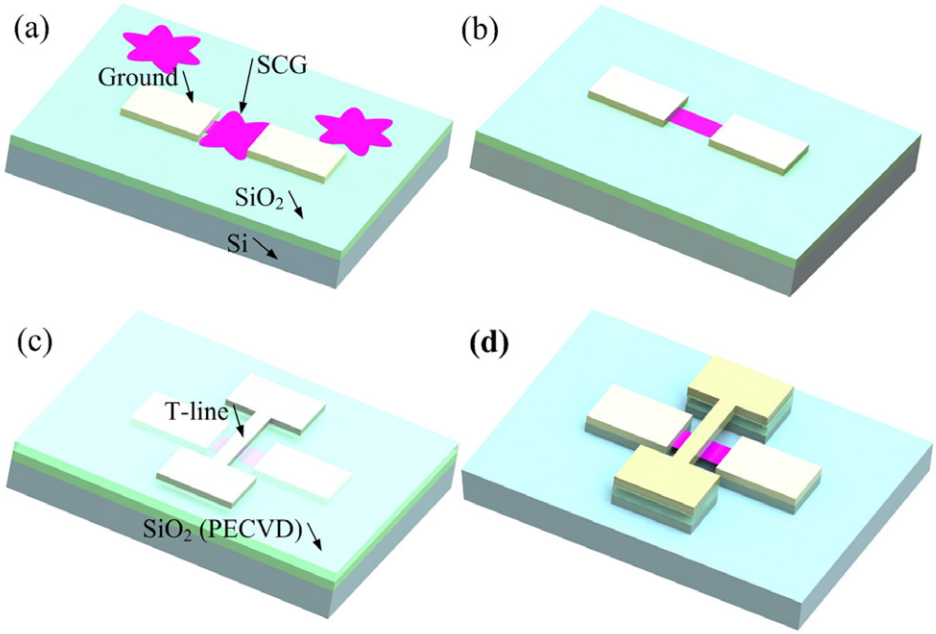

Figure 2. SCG RF switch fabrication process. (a) Transfer SCG on SiO_2/Si substrate and fabricate metal electrode (ground electrodes) by lift-off process. (b) Etch SCG into rectangular beam shape by O_2 plasma dry etching. (c) Deposit SiO_2 on top of the sample by PECVD and fabricate top electrode (T-line). (e) Etch SiO_2 with buffered oxide etch (BOE) to release SCG beam and T-line.

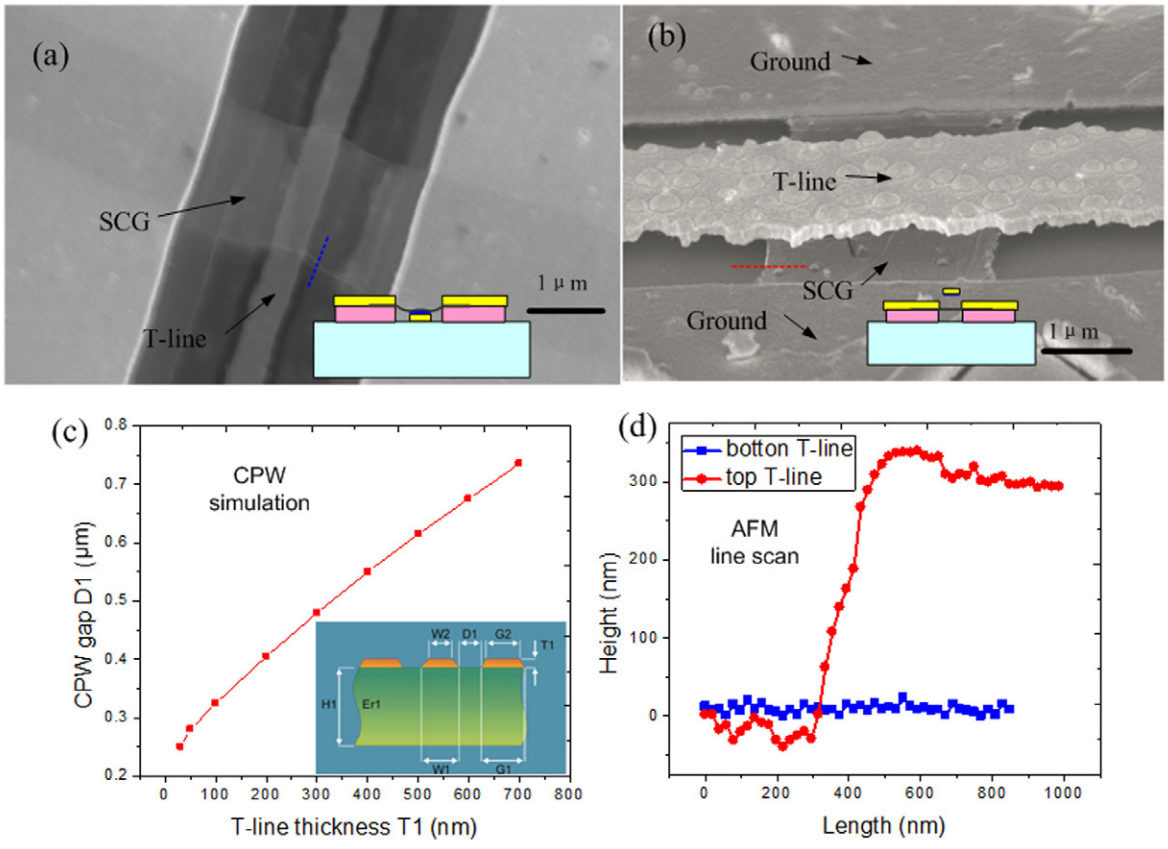

Figure 3. (a) SCG RF NEMS switch with the T-line beneath SCG. The SCG beam collapsed onto the substrate after fabrication because of the metal fence effect. (b) SCG switch with T-line on top of suspended SCG. (c) Relation between T1 (T-line thickness) and D1 (lateral distance between T-line and ground electrode) (simulation result). Impedance of CPW is 50 Ω. Thickness of T-line (T1) should be at least in the order of hundreds of nanometers; otherwise, lateral distance between T-line and ground electrode (D1) will be too small to be patterned by regular photolithography. (d) AFM line scans. The blue and red dashed lines in (a) and (b) show the scan distance. The AFM height curve demonstrates that the SCG beam is suspended in (b) and collapsed onto the substrate in (a).

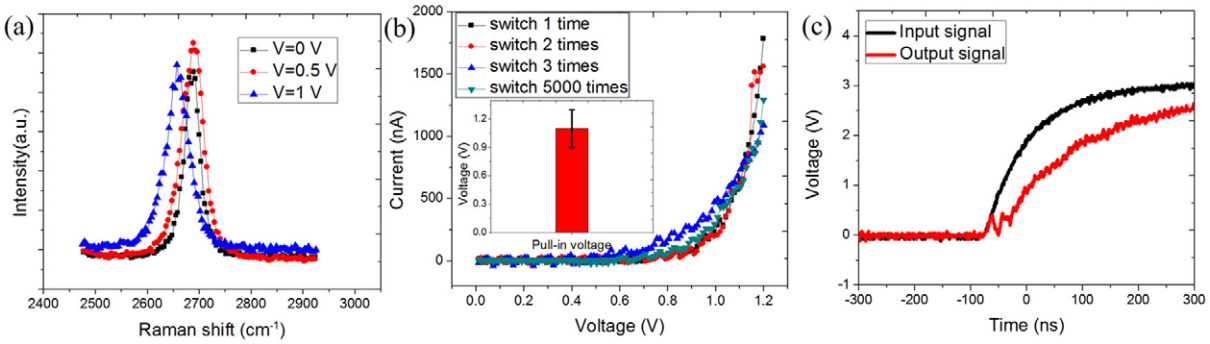

Figure 4. (a) Pull-in voltage of SCG RF NEMS switch detected by RSM. Red shift of G peak was observed when the bias exceeds 1 V, indicating the value of pull-in voltage. (b) *I–V* curves of SCG switch operating 1, 2, 3 and 5000 times, respectively. The inset shows the dispersion of the pull-in voltage. (c) The switching speed of the SCG switch derived from the time difference between input and output signal which is on the order of nanoseconds.

This high carrier mobility is comparable to or even larger than that of CVD SCG reported in the literature (~ 5200 $cm^2 V^{-1} s^{-1}$ [12]). The I_{DS} versus V_{GS} curve also indicates that the conductance of graphene film, R_{DS}, can be tuned by the bias V_{GS}, which can affect the RF performance of a graphene NEMS switch.

SCG RF NEMS switches integrated with coplanar wave guide were fabricated with micromanufacture processes. The coplanar waveguide (CPW) is consisted of two ground electrodes with a transmission line (T-line) in between. It can reduce the loss effectively during RF signal transmission [25]. One of the star-like shaped monolayer SCGs was chosen to fabricate the switch. After the SCG transfer process, some flakes had cracks or ripples, and some overlapped. Those SCGs were not chosen for device fabrication. Ground electrodes were defined by photolithography, followed by image reverse technique (after UV light exposure, the samples were baked in an oven filled with ammonia. As a result, the positive photoresist acted as negative, and only the UV-exposed parts were covered with photoresist), electron-beam evaporation, and metal lift-off (figure 2(a)). The SCG was etched into the rectangular beam by O_2 plasma dry etching (figure 2(b)). The CPW impedance value should be equal to 50 Ω. Therefore, according to simulation results (figure 3(c)), the thickness of the T-line (T1) should be at least on the order of hundreds of nanometers; otherwise, the lateral distance between the T-line and the ground electrode (D1) will be too small to be patterned by regular photolithography. We first tried to place the thick T-line beneath the SCG beam. As a result, a high metal fence at the edge of T-line led to serious stiction problems after etching the SiO_2 sacrificial layer (figure 3(a)), since the discontinuous surface topography increased the length of the SCG beam. To resolve this problem, we proposed a new structure, fabricating the T-line after SCG transferring process (figure 3(b)). Therefore, the SCG film is completely flat, and the metal fence effect can be avoided. Additionally, the location of the SCG is hard to control precisely during the transferring process. Therefore, patterning the T-line according to the position of SCG after the graphene-transferring process is a more efficient way to fabricate the device. A buffered oxidize etcher was applied to etch SiO_2 and release the free-standing structure, followed by critical point drying to reduce the chance of stiction. The suspension of the SCG beam was verified by AFM measurement (figure 3(d)). The AFM height curve demonstrates that the distance between the suspended SCG beam and the Si substrates is equal to 300 nm, which is the thickness of the SiO_2 sacrificial layer. The yield of fabrication is 7 out of 10 devices. The principal cause of failure in our device was due to stiction after critical point drying.

Electromechanically actuated RF NEMS switches based on SCG were investigated. SCG film can be pulled up to be in contact with the T-line when applying a dc voltage larger than threshold voltage (pull-in voltage) between the T-line and SCG beam. On the contrary, the contact will be broken by an elastic force after the bias is removed. Pull-in voltage of the NEMS switch is given by

$$V_{\text{pull-in}} = \sqrt{\frac{8kg_0^3}{27\varepsilon A}}, \tag{2}$$

where k is the spring constant of SCG beam, g_0 is the gap between the beam and the T-line, ε is the effective permittivity, and A is the size of the suspended SCG beam beneath the T-line. The spring constant k of a fixed-end beam with a distributed load is [26]

$$K = 32Ew(t/\ell)^3, \tag{3}$$

where E is the Young's modulus of graphene and w, t, and ℓ are the width, thickness, and length of the graphene beam. The spring constant of our SCG beam is about 65 μN m^{-1}. The Raman spectra method (RSM) [27] was applied to measure the pull-in voltage of the capacitive shunt switch. A sudden red shift of the Raman G peak was observed when the bias was over 1 V (figure 4(a)), which is caused by the strain in the SCG membrane due to large deformation, indicating the pull-in voltage is 1 V. When the bias (0.5 V) was smaller than pull-in voltage, the 2D peak did not have obvious shift, indicating the shift was mainly due to the deformation of the beam rather than gate electrostatic doping. We also tested the switch without isolation layer with the I–V method. Once applied, bias is larger than the pull-in voltage (1 V), a sharp increase of the current will be observed, which indicates that the switch is turned on (figure 4(b)). Pull-in voltages of seven devices with the same geometry size were tested, and the dispersion

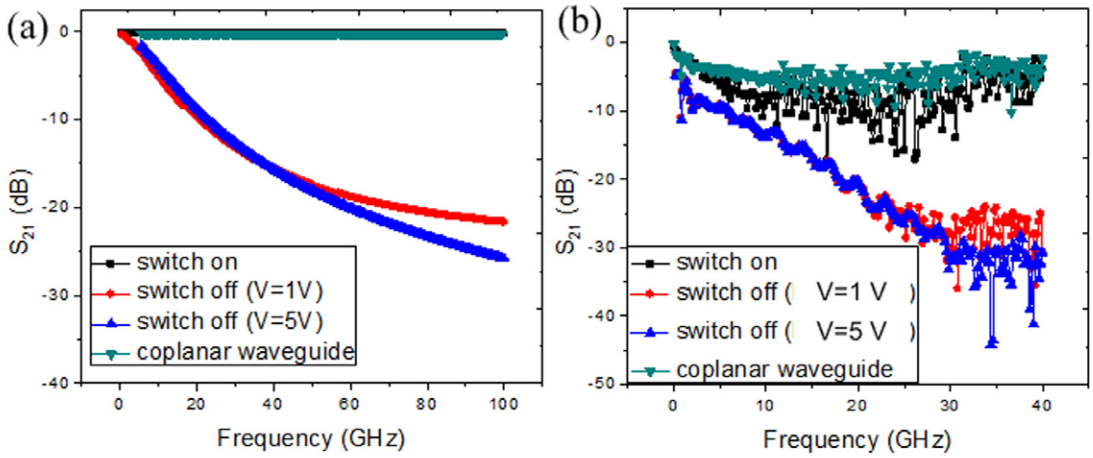

Figure 5. (a) S_{21} parameter simulation results of SCG RF switch at on-state and off-state, respectively, from 0 Hz to 100 GHz. (b) S_{21} parameter experimental results of SCG RF switch at on-state and off-state, respectively, from 0 Hz to 40 GHz. When the switch is turned off, increasing bias can result in better isolation.

of pull-in voltage values is shown in figure 4(b). Our SCG switch's pull-in voltage is much smaller than that of conventional RF MEMS switches and it is compatible with MOS circuit requirements. Lifetime (dc actuation times) limited by fracture failure limits the application of graphene actuators (switches and resonators). The polycrystalline graphene switch is reported to operate only 4–5 times due to the grain boundary defect [1, 28]. Without the influence of the grain boundary, our SCG switches switched 5000 times without failure, as demonstrated in figure 4(b), showing lifetimes much longer than those of polycrystalline graphene switches reported in literature.

Switching speed is another important parameter. For electromechanically actuated switches, switching time consists of response time, which is the time required to overcome mechanical inertia, and rise time of the voltage pulse due to charging capacitance. The switching time, t, is given by [29]

$$t = \frac{3.67 V_{\text{pull-in}}}{2\pi f_0 V}, \tag{4}$$

where V is the step function voltage and f_0 is the first-order resonant frequency of the beam. In general, conventional MEMS/NEMS has a switching time in the microsecond regime. However, the high Young's modulus and extremely low mass density of graphene result in ultra-high resonant frequency and switching speed. The switching speed of our SCG switch was characterized by applying a step signal to the device input terminals, while the output signal was measured concurrently, as shown in figure 4(c). The time difference between these two signals indicates the possibility of operating a SCG switch in nanosecond regime.

The RF properties of SCG switches were investigated by measuring the scattering parameters (S-parameters). S_{21} is the amplitude ratio of output and input RF signals. When the SCG beam is in the down state, the switch is turned on. RF signal can pass through the switch from the T-line without apparent damping. Therefore, $S_{12} = 0$ dB is expected for an ideal RF NEMS switch when it is on. Figure 5(b) demonstrates that S_{21} for our switch is approximately −6 dB. This reduction of S_{21} is owing to loss from the Si substrate, the PECVD SiO_2 layer, and the coplanar waveguide. We tested the solely coplanar waveguide, and S_{21} of about −4 dB was derived. We assume the high surface roughness of the T-line (figure 3(b)) is mainly responsible for the high-frequency loss of CPW. When the SCG beam is pulled up and contacts the T-line, the RF switch is turned off, forming a low-impedance RF short cut path to the ground. S_{21} value represents isolation when the RF switch is turned off [29]. Better conductance of the beam is responsible for better isolation of the RF switch [29]. Polycrystalline graphene has 1 order larger resistance across the grain boundary [8], thus SCG devices can obtain better isolation. The isolation of our SCG switch detected can reach −30 dB at 40 GHz (Ka band). This value is comparable to silicon-based RF switches [30]. Interestingly, when we further increased the bias after the switch was turned off, an even smaller S_{21} value was observed. We assume this is due to graphene's unique electric field effect (figure 1(c)). Larger bias increases the conductance of SCG beam, resulting in better isolation. It is consistent with our simulation results in figure 5(a).

3. Conclusion

LPCVD was applied to derive monolayer SCG by controlling growth duration. Raman, AFM, and carrier mobility measurements demonstrate the high quality and single-crystal nature of the samples. A new structure of RF switch is proposed to solve the 'metal fence' effect. SCG switches are able to operate at a very low actuation voltage and fast switching speed. The devices exhibits lifetime of over 5000 cycles without a breakdown, superior to polycrystalline graphene NEMS switches reported. The devices demonstrate superb isolation (−30 dB at 40 GHz (Ka band)), which can be further improved by SCG's conductivity variation due to actuation voltage. The results presented here suggest that CVD SCG is an excellent candidate for RF NEMS switches.

Acknowledgments

The work described in this paper was supported by the National Natural Science Foundation of China (No 51405257) and the Science Fund of China Post Doctor (No 2012M520259). The authors acknowledge the assistance of fabrication and characterization by the Minnesota Nano Center and Characterization Facility at the University of Minnesota.

References

[1] Milaninia K M, Baldo M A, Reina A and Kong J 2009 All graphene electromechanical switch fabricated by chemical vapor deposition *Appl. Phys. Lett.* **95** 183105

[2] van der Zande A M, Barton R A, Alden J S, Ruiz-Vargas C S, Whitney W S, Pham P H Q, Park J, Parpia J M, Craighead H G and McEuen P L 2010 Large-scale arrays of single-layer graphene resonators *Nano Lett.* **10** 4869–73

[3] Chakraborty A, Gupta B and Sarkar B K 2014 Design, fabrication an characterization of miniature RF MEMS switched capacitor based phase shifter *Microelectron. J.* **45** 1093–102

[4] Badzey R, Zolfagharkhani G, Gaidarzhy A and Mohanty P 2004 A controllable nanomechanical memory element *Appl. Phys. Lett.* **85** 3587–9

[5] Novoselov K S, Geim A K, Morozov S V, Jiang D, Zhang Y, Dubonos S V, Grigorieva I V and Firsov A A 2004 Electric field effect in atomically thin carbon films *Science* **306** 666–9

[6] Lee C, Wei X, Kysar J W and Hone J 2008 Measurement of the elastic properties and intrinsic strength of monolayer graphene *Science* **321** 385–8

[7] Li X *et al* 2009 Large-area synthesis of high-quality and uniform graphene films on copper foils *Science* **324** 1312–4

[8] Yu Q *et al* 2011 Control and characterization of individual grains and grain boundaries in graphene grown by chemical vapour deposition *Nat. Mater.* **10** 443–9

[9] Li X *et al* 2010 Graphene films with large domain size by an two-step chemical vapor deposition process *Nano Lett.* **10** 4328–34

[10] Wu Y A, Fan Y, Speler S, Creeth G L, Sadowski J T, He K, Robertson A W, Allen C S and Warner J H 2012 Large single crystals of graphene on melted copper using chemical vapor deposition *ACS Nano* **6** 5010–7

[11] Hao Y *et al* 2013 The role of surface oxygen in the growth of single-crystal graphene on copper *Science* **342** 720–3

[12] Chen S, Ji H, Chou H, Li Q, Li H, Suk J W, Piner R, Liao L, Cai W and Ruoff R S 2013 Millimeter-size single-crystal graphene by suppressing evaporative loss of Cu during low pressure chemical vapor deposition *Adv. Mater.* **25** 2062–5

[13] Yan Z, Lin J, Peng Z W, Sun Z Z, Zhu Y, Li L, Xiang C S, Samuel E L, Kittrell C and Tour J M 2013 Toward the synthesis of wafer-scale single-crystal graphene on copper foils *ACS Nano* **7** 2872

[14] Kim K S, Zhao Y, Jang H, Lee S Y, Kim J M, Kim K S, Ahn J H, Kim P, Choi J Y and Hong B H 2009 Large-scale pattern growth of graphene films for stretchable transparent electrodes *Nature* **457** 706–10

[15] Gao L *et al* 2012 Repeated growth and bubbling transfer of graphene with millimeter-size single-crystal grains using platinum *Nat. Commun.* **3** 699

[16] Yagi K, Yamada A, Hayashi K, Harada N, Sato S and Yokoyama N 2013 Dependence of field-effect mobility of graphene grown by thermal chemical vapor deposition on its grain size *Japan. J. Appl. Phys.* **52** 1100106

[17] Lee G H *et al* 2013 High-strength chemical-vapor-deposited graphene and grain boundaries *Science* **340** 1073–6

[18] Rasool H I, Ophus C, Klug W S, Zettl A and Gimzewski J K 2013 Measurement of the intrinsic strength of crystalline and polycrystalline graphene *Nat. Commun.* **4** 2811

[19] Sharma P, Perruisseau-Carrier J, Moldovan C and Ionescu A M 2014 Electromagnetic performance of RF NEMS graphene capacitive switches *IEEE Trans. Nanotechnol.* **13** 70–9

[20] Sharma P, Perruisseau-Carrier J and Ionescu A M 2013 Nanoelectromechanical microwave switch based on graphene *14th Int. Conf. on Ultimate Integration on Silicon (ULIS, Coventry, UK 19–21 March)* pp 190–3

[21] Jang M W *et al* 2011 A pure single-walled carbon nanotube thin film based three-terminal microelectromechanical switch *Appl. Phys. Lett.* **98** 073502

[22] Cheng Z, Zhou Q, Wang C, Li Q, Chen W and Fang Y 2011 Toward intrinsic graphene surfaces: a systematic study on thermal annealing and wet-chemical treatment of SiO_2-supported graphene devices *Nano Lett.* **11** 767–71

[23] Liu C, Liu L, Mak K F, Flynn G W and Heinz T F 2009 Ultraflat graphene *Nature* **462** 339–41

[24] Liang X, Fu Z and Chou S Y 2007 Graphene transistors fabricated via transfer-printing in device active-areas on large wafer *Nano Lett.* **7** 3840–4

[25] Yao J J 2000 RF MEMS from a device perspective *J. Micromech. Microeng.* **10** R9–38

[26] Li P, You Z, Haugstad G and Cui T 2011 Graphene fixed-end beam arrays based on mechanical exfoliation *Appl. Phys. Lett.* **98** 253105

[27] Li P, You Z and Cui T 2012 Raman spectrum method for characterization of pull-in voltages of graphene capacitive shunt switches *Appl. Phys. Lett.* **101** 263103

[28] Kim S M, Song, E B, Lee S, Seo S, Seo D, Hwang Y, Candler R and Wang K L 2011 Suspended few-layer graphene beam electromechanical switch with abrupt on-off characteristics and minimal leakage current *Appl. Phys. Lett.* **99** 023103

[29] Rebeiz F M 2003 *RF MEMS Theory, Design, and Technology* (Hoboken, NJ: Wiley)

[30] Zhu Y Q, Qian H, Wang L F and Tang J Y 2014 Measurement and analysis of substrate leakage current of RF mems capacitive switches *Microelectron. Reliab.* **59** 152–9